Hydrogen-Embrittled Fracture of Dual Phase High-Strength Steel Sheets with Different Microstructural Hardness

KEI SAITO (1) , MASAHIKO DEMURA (2) , KENICHI TAKAI (*) (3)

(1) Graduate School of Science and Technology, Sophia University, now at National Institute for Materials Science, Japan

(2) National Institute for Materials Science, Japan

(3) Faculty of Science and Technology, Sophia University, Japan

(*) *(corresponding author)*
takai-k@sophia.ac.jp

ABSTRACT

Advanced-high strength steels (AHSS) have been attracting attention in recent years for application to structure parts of automobile to secure both crashworthiness and weight reductions. Developing AHSS with excellent resistance to hydrogen embrittlement (HE) is an urgent issue since the risk of HE increases with increase in a tensile strength of steel due to hydrogen uptake under vehicle manufacturing process and market service. The present study aimed to elucidate the effect of microstructural hardness on resistance to hydrogen embrittlement in ferrite-martensite dual-phase (DP) steel sheet with a tensile strength of approximately 1180 MPa. Two kinds of DP specimens with similar tensile strength, but different microstructural hardness between ferrite and martensite, were prepared: as-quenched DP (DP-AQ) and tempered DP (DP-TM) specimens with a high and low difference in microstructural hardness, respectively. The resistance to HE of two types of specimens was evaluated by using slow strain rate tensile test (SSRT) *in-situ* a specific electrochemical charging with hydrogen, based on the change in the maximum fracture strength and uniform elongation obtained by stress-strain curves, and fracture strain calculated by the amount of reduction in area. The maximum fracture strength was similar among hydrogen-charged two types of specimens. The orders of uniform elongation and fracture strain for the hydrogen-charged two types of specimens were DP-TM > DP-AQ. The fracture surface of hydrogen-charged DP-AQ specimen was mainly quasi-cleavage over the entire fracture surface, however that of DP-TM specimen was quasi-cleavage only around the crack initiation site and dimple patterns was observed apart from crack initiation area. These results indicate that reduction in microstructural hardness between ferrite and martensite improves the HE resistance in terms of global and local ductility due to presumably suppressing the hydrogen-related crack initiation and crack propagation in brittle mode.

KEYWORDS

hydrogen embrittlement
dual phase steel
hardness
ductility

1. INTRODUCTION

The application of advanced high-strength steels (AHSS) with tensile strength exceeding 1180 MPa to structural components of the automobile body has been expanding to achieve both weight reductions and greater crashworthiness. However, it is well known that as the strength of steel increases, so does the risk of hydrogen embrittlement (HE) caused by trace amounts of hydrogen induced during the vehicle manufacturing process or from the service environment. Therefore, establishing effective strategies to enhance the HE resistance of AHSS has become an urgent issue. In dual-phase (DP) steels, a representative AHSS, mechanical properties such as strength, ductility [1], and crack propagation behavior [2] can be significantly altered by varying the hardness and volume fraction of the ferrite and martensite phases. HE is known to be a phenomenon closely related to localized plastic deformation in metals [3]. In DP steels, it is considered that the development of localized plasticity between the two phases with different mechanical properties plays a critical role in governing their susceptibility to HE. Although the HE susceptibility [4] and the mechanism of hydrogen-related crack initiation [5] in DP steels with various tensile strengths have been studied, there have been no studies that examined the effect of the difference in hardness between the ferrite and martensite phases on the HE behavior of DP steels with similar tensile strength. The aim of this study was to clarify the effect of hardness differences between the ferrite and martensite phases on HE susceptibility and fracture morphologies by using DP steels with similar tensile strength of approximately 1180 MPa, but different microstructural hardness.

2. EXPERIMENTAL

2.1 Materials

Two types of DP steel sheets with a tensile strength of approximately 1180 MPa and a thickness of 1.0 mm were fabricated by applying different heat treatment conditions to a commercial high-strength automotive steel sheet (JFS-JSC1180Y), in order to vary the hardness difference between the ferrite and martensite phases. An as-quenched type, denoted as DP-AQ, was produced by water quenching from 750□ °C, resulting in a high hardness difference between ferrite and martensite. A tempered type, referred to as DP-TM, was obtained by water quenching from 770□ °C followed by tempering at 200□ °C, which reduced the hardness difference between the two phases.

Figure 1 shows the nominal stress versus nominal strain curves for the two types of steel obtained in a uniaxial tensile test conducted in air with a contact-type extensometer. Figure 2 presents the microstructures of the two types of steels etched with a 3 vol.% nital solution, followed by observation using a field emission scanning electron microscope (FE-SEM). Microstructural hardness was evaluated in a micro-Vickers hardness test. A load of 0.01 kgf was applied, and measurements were conducted on specimens the microstructure of which was exposed by etching. Ten indentations were made in each of the ferrite and martensite regions, and the average of the middle eight values, excluding the maximum and minimum ones, was taken to represent the hardness of each phase. Table 1 summarizes the mechanical properties and microstructural characteristics of the two types of steel.

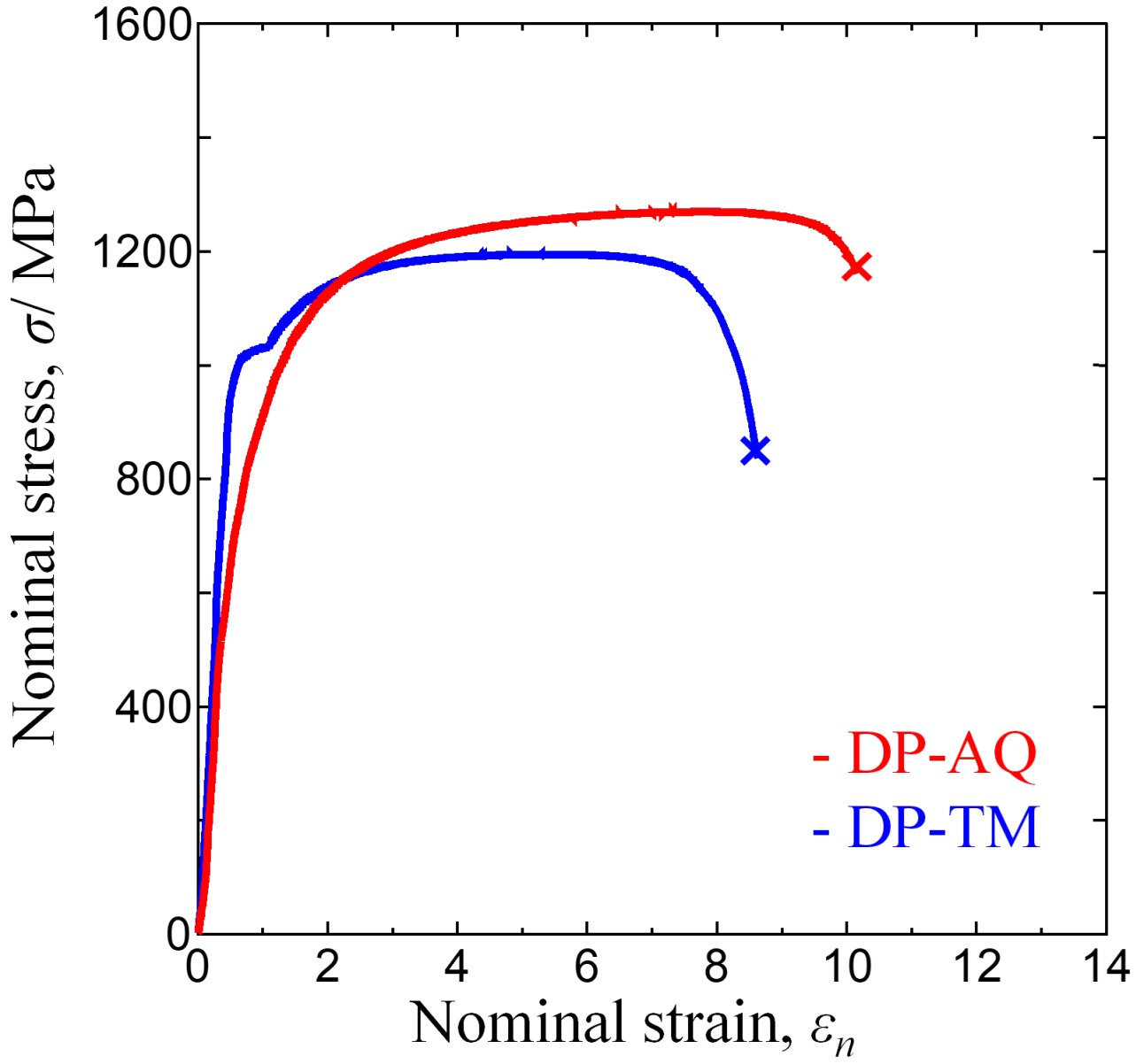

Figure 1 - Nominal stress versus nominal strain curves of the two types of specimens obtained with an extensometer in tensile tests.

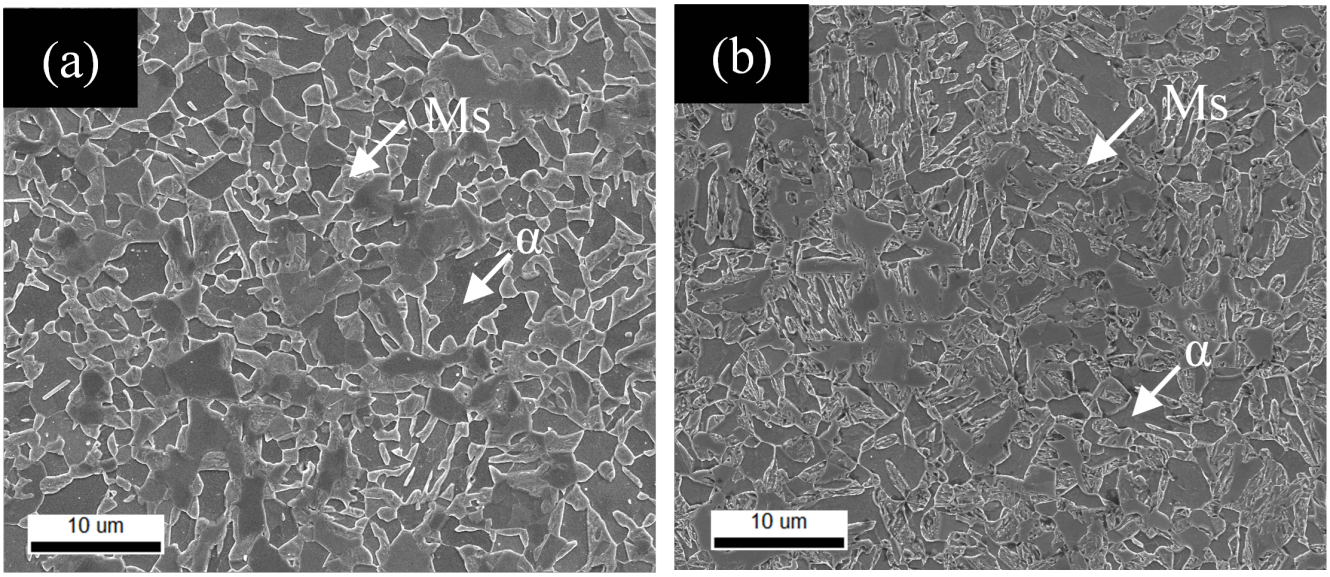

Figure 2 - Microstructure of the two types of specimens as observed by FE-SEM: (a) DP-AQ and (b) DP-TM

Table 1 - Mechanical and microstructural properties of the two types of specimens: YS, TS, U-EL, and T-EL represent 0.2% proof stress, tensile strength, uniform elongation, and total elongation, respectively. α and Ms mean ferrite and martensite, respectively.

	Mechanical properties				Phase properties	
	0.2% PS (MPa)	TS (MPa)	U- EL (%)	T-EL (%)	Vickers hardness (0.1HV)	
					α	Ms
DP-AQ	756	1269	7.8	10.2	204	445
DP-TM	1014	1195	5.3	8.6	243	363

2.2 Hydrogen charging and hydrogen analysis

Hydrogen pre-charging was performed by cathodic electrolysis at a constant current density of 5.0 $A \cdot m^{-2}$ for 96 hours in an aqueous solution of 0.1 $mol \cdot L^{-1}$ NaOH containing 1.0 $g \cdot L^{-1}$ NH_4SCN at 30 °C. This procedure ensured a uniform hydrogen concentration between the surface and center of the specimen in the thickness direction. Hydrogen charging was conducted on flat specimens with a width of 7 mm and a length of 20 mm.

The hydrogen content was analysed using a thermal desorption analyzer (TDA) equipped with a gas chromatograph having a semiconductor detector. Following hydrogen charging, the specimens were quenched in liquid nitrogen and then subjected to TDA at a heating rate of 100 $°C \cdot h^{-1}$ over a temperature range of 0 to 300 °C.

2.3 Slow strain rate tests

Flat tensile specimens with a parallel gauge section 20 mm long and 7 mm width were prepared. After pre-charging hydrogen into the gauge section, slow strain rate tensile tests (SSRTs) were conducted under continuous hydrogen charging at a

crosshead speed of 0.012 mm·min⁻¹. For comparison, SSRTs were also performed at 30 °C in an isothermal chamber without hydrogen charging.

The fracture surfaces were observed by field emission scanning electron microscopy (FE-SEM). The fracture strain (εf) was calculated using the initial cross-sectional area (A_0) before the SSRT and the final fracture surface area (A_f), as expressed in Equation (1):

$$\varepsilon_f = \ln(A_0/A_f) \quad (1)$$

After the SSRT, the hydrogen content remaining in the fractured specimens was also quantified by TDA.

3. RESULTS AND DISCUSSION

Figure 3 shows the nominal stress versus displacement curves for the two steel types with and without hydrogen charging. For both steels, a significant loss of ductility was observed in hydrogen-charged specimens compared with non-charged ones. Figure 4 presents the fracture morphologies of the two steels with hydrogen charging after the SSRT, as observed by FE-SEM. Figures 4(a) and 4(b) show the overall fracture morphology, while Figs. 4(c) and 4(d) provide magnified views of the crack initiation areas marked by white squares in Figs. 4(a) and 4(b), respectively. Figure 4(e) presents a magnified view of the area far from the crack initiation area. As shown in Fig. 4(a), the DP-AQ specimen exhibited almost no necking across the entire fracture surface. A quasi-cleavage fracture surface characterized by flat facets was observed, as indicated by the contrast in the SEM image in Fig. 4(c). In contrast, although the crack initiation region in

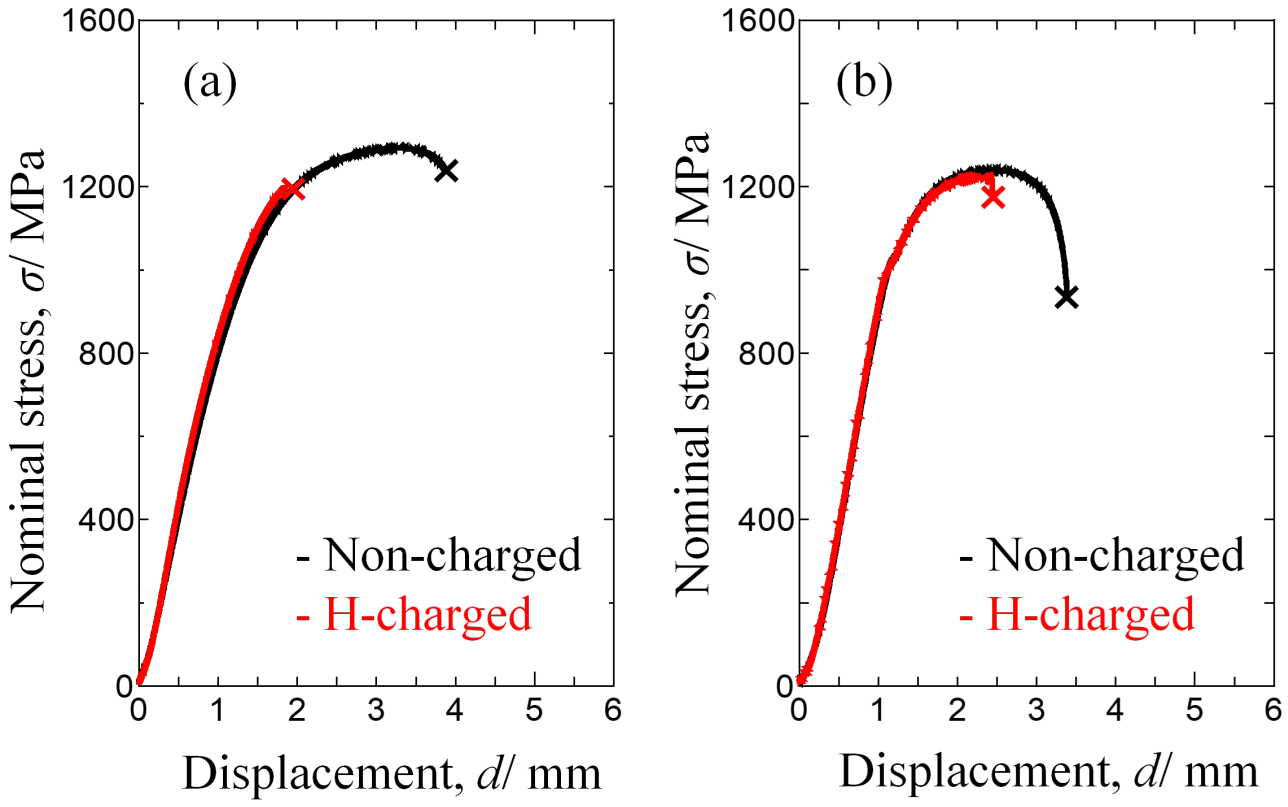

Figure 3 - Nominal stress versus displacement curves of the two types of specimens with/without hydrogen charging obtained by slow strain rate tensile testing: (a) DP-AQ, (b) DP-TM.

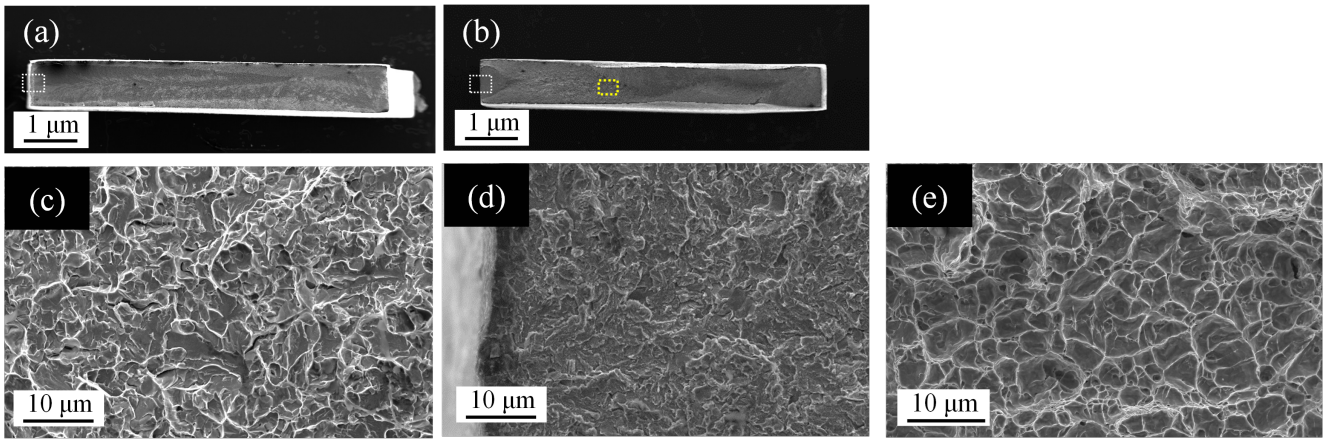

Figure 4 - Fracture morphologies of the two types of hydrogen-charged specimens as observed by FE-SEM: (a)(c) DP-AQ and (b)(d) DP-TM. (c)(d) magnify the region surrounded by white rectangles in (a)(b) respectively and (e) magnifies the region surrounded by yellow rectangle in (b).

the DP-TM specimen, marked by the white square in Fig. 4(b), also exhibits a typical quasi-cleavage fracture surface. However, in the region far from the initiation area, necking is evident. As shown in Fig. 4(e), a dimpled fracture surface with pronounced roughness is observed, which is presumably due to the coalescence of voids.

Figure 5 shows the (a) maximum fracture strength, (b) uniform elongation, and (c) fracture strain of the two steels obtained by the SSRT with/without hydrogen charging. Figure 5(d) presents the hydrogen content measured by TDA both after hydrogen pre-charging and after the SSRT. As shown in Fig. 5(a), the maximum fracture strength of both steels exhibited no significant change upon hydrogen charging compared with the uncharged condition. In contrast, Fig. 5(b) indicates that hydrogen charging markedly reduced the uniform elongation of the DP-AQ specimen, whereas that of the DP-TM specimen decreased only slightly. In Fig. 5(c), it is evident that the fracture strain of the hydrogen-charged DP-TM and DP-AQ specimens decreased significantly compared with that of the non-charged specimens. According to Fig. 5(d), the initial hydrogen content of the two steels was comparable, at approximately 0.23 ppm for DP-AQ specimen and 0.13 ppm for DP-TM specimen. However, after the SSRT, the hydrogen content increased to 0.43 ppm for DP-AQ specimen and 0.96 ppm for DP-TM specimen.

These results show that reducing the hardness difference between ferrite and martensite, as in the DP-TM specimen, effectively enhanced resistance to HE, particularly by mitigating the hydrogen-induced degradation in uniform elongation.

Hydrogen-related microcracking in DP steels has been documented to occur not only within the martensitic phase but also at the interfaces between ferrite and martensite [4] . Such microcracks are considered to be initiated by localized strain concentrations arising from the mechanical incompatibility at these phase boundaries, compounded by the hydrogen-induced degradation of interfacial cohesion [4, 6] . Moreover, it has been reported that microcracks may develop within the uniform elongation regime even in the absence of

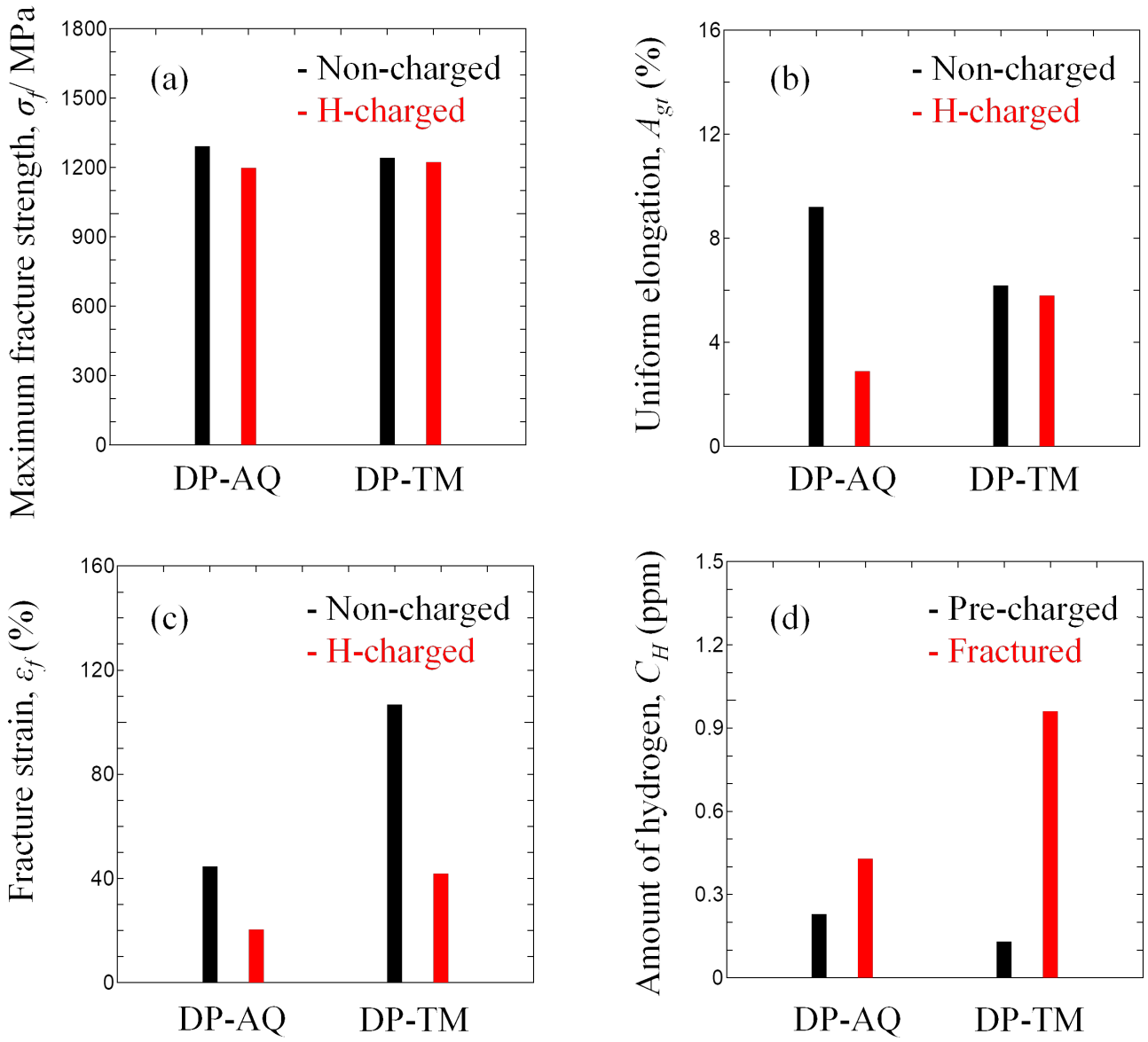

Figure 5 - (a) Maximum fracture strength, (b) uniform elongation, and (c) fracture strain of the two types of specimens with/without hydrogen charging as obtained by SSRT and (4) amount of hydrogen of pre-charged specimens and fractured specimens after SSRT as measured by TDA.

hydrogen [7] . In light of these observations, it can be postulated that the reduction of the hardness difference between ferrite and martensite mitigated strain localization at the phase interfaces, thereby suppressing the nucleation of hydrogen-related microcracks.

Consequently, the threshold for rapid propagation of hydrogen-induced cracking increased, which plausibly accounts for the slight decrease in uniform elongation in the DP-TM specimen under hydrogen-charging conditions.

On the other hand, as shown in Fig. 5(c), the fracture strain of DP-TM specimen under hydrogen-charged SSRT is higher than that of DP-AQ specimen; however, it still decreases significantly compared to the uncharged condition. This result is attributed to the fact that, as shown in Fig. 5(d), DP-TM specimen exhibits a higher threshold uniform elongation under hydrogen charging than DP-AQ specimen, resulting in a greater amount of hydrogen ingress during SSRT, which consequently accelerates crack propagation.

4. CONCLUSIONS

In this study, dual-phase steels with similar tensile strength but different hardness differences between ferrite and martensite were evaluated for hydrogen embrittlement susceptibility using SSRT and their fracture surfaces were observed by FE-SEM. The following findings were obtained:

- The maximum fracture strength of the two steels showed negligible change regardless of hydrogen charging. However, the uniform elongation of DP-AQ specimen significantly decreased under hydrogen charging, whereas that of DP-TM specimen exhibited only a slight reduction. Furthermore, the fracture strain during SSRT *in-situ* hydrogen charging was higher in DP-TM specimen than in DP-AQ specimen.
- Quasi-cleavage fracture surfaces were observed around the crack initiation sites in both DP-AQ and DP-TM specimens. Away from the initiation region, the fracture morphology of DP-AQ specimen was also the quasi-cleavage fracture mode, while the fracture surface of DP-TM specimen exhibited necking, indicating the presence of ductile fracture.

These results demonstrate that reducing the hardness difference between the ferrite and martensite phases in DP steels can effectively enhance resistance to hydrogen embrittlement.

ACKNOWLEDGEMENTS

This work was supported by JSPS KAKENHI Grant Number JP24K21211.

REFERENCES

[1] H. Mohrbacher and NiobelCon bvba, Advanced metallurgical concepts for DP steels with improved formability and damage resistance, Proceedings of the international symposium on new developments in advanced high-strength sheet steels, Vail, AIST, (2013). https://doi.org/10.33313/298%2F015

[2] C. C. Tasan, M. Diehl, D. Yan, M. Bechtold, F. Roters, L. Schemmann, C. Zheng, N. Peranio, D. Ponge, M. Koyama, K. Tsuzaki, and D. Raabe, An Overview of Dual-Phase Steels: Advances in Microstructure-Oriented Processing and Micromechanically Guided Design, Annu. Rev. Mater. Res., 45 (2015) 391. https://doi.org/10.1146/annurev-matsci-070214-021103

[3] M.L. Martin, M. Dadfarnia, A. Nagao, S. Wang, P. Sofronis, Enumeration of the hydrogen-enhanced localized plasticity mechanism for hydrogen embrittlement in structural materials, *Acta Mater*. 165 (2019) 734. https://doi.org/10.1016/j.actamat.2018.12.014

[4] M. Koyama, C. C. Tasan, E. Akiyama, K. Tsuzaki, D. Raabe, Hydrogen-assisted decohesion and localized plasticity in dual-phase steel, *Acta Mater*., 70 (2014) 174. https://doi.org/10.1016/j.actamat.2014.01.048

[5] E. Rodoni, K. Verbeken, T. Depover, M. Iannuzzi, Effect of microstructure on the hydrogen embrittlement, diffusion, and uptake of dual-phase low alloy steels with varying ferrite-martensite ratios, Int. J. Hydro. Energ., 50 (2023) 53. https://doi.org/10.1016/j.ijhydene.2023.07.061

[6] D. Asari, S. Mizokami, M. Fukahori, K. Takai, Microscopic defects formed during crack incubation, initiation and propagation processes causing hydrogen-related fracture of dual-phase steels, *Mater. Sci. & Eng. A*, 780 (2020) 139209. https://doi.org/10.1016/j.msea.2020.139209

[7] H. Toda, A. Takijiri, M. Azuma, S. Yabu, K. Hayashi, D. Seo, M. Kobayashi, K. Hirayama, A. Takeuchi, K. Uesugi., Damage micromechanisms in dual-phase steel investigated with combined phase- and absorption-contrast tomography, *Acta Mater.*, 126 (2017) 401. https://doi.org/10.1016/j.actamat.2017.01.010